Physical and observational constraints on the anvil cloud feedback

Brett A. McKim[a,b,1], **Sandrine Bony**[a], **and Jean-Louis Dufresne**[a]

[a]LMD/IPSL, Sorbonne Université, CNRS, 75252 Paris, France; [b]University of Exeter, Stocker Rd, EX4 4PY Exeter, UK

This manuscript was compiled on February 28, 2023

Changes in anvil cloud area with warming are one of the largest sources of uncertainty in Earth's climate sensitivity (Sherwood et al 2020). Here, we develop a simple theory of cloud radiative effects and derive an equation for the tropical anvil cloud area feedback. Our theory shows that the feedback is given by the product of the present day (and thus measurable) cloud radiative effect and the fractional change in anvil area with warming. Satellite observations suggest a cloud radiative effect ≈ -1 Wm^{-2} and a sensitivity of anvil clouds to surface temperature $\approx -11\%$ K^{-1} at the interrannual time scale (Saint-Lu et al, 2020), leading to a tropical anvil cloud area feedback of 0.08 ± 0.05 Wm^{-2}K^{-1}. This feedback is thus weaker and better constrained than previously thought. We then use our theory to derive an equation for the proportionally higher anvil temperature feedback, which depends on the change in anvil temperature with warming. Satellite observations suggest this change is ≈ 0.44 K K^{-1}. Combining the resultant temperature feedback with the area feedback leads to a total anvil cloud feedback of -0.01 ± 0.09 Wm^{-2}K^{-1}. Changes in anvil clouds with warming appear to have little effect on climate sensitivity.

anvil clouds | cloud feedbacks | climate sensitivity | climate change

Anvil clouds are the cirrus cover formed by detrainment from deep convection. Anvils blanket the tropics and modify Earth's energy balance by reflecting sunlight and trapping infrared radiation. Their reduction in area with warming (1, 2) is a leading source of uncertainty in estimating climate sensitivity (3), and given new constraints on low cloud feedbacks (4, 5), the anvil cloud area feedback is now the most uncertain cloud feedback of all. But can it be better constrained?

Changes in anvil clouds with warming

Ramanathan and Collins (6) first explored the idea that changing anvil cloud cover could alter Earth's climate sensitivity by regulating ocean surface temperature like a thermostat. However, the drop off in frequency of both deep convection and surface temperature above a certain threshold temperature are no longer considered evidence of a tropical thermostat (7–10). Ten years later, Lindzen et al (11), through a different chain of logic, reasoned that reduced anvil cloud cover with warming could act like a shrinking iris and significantly dampen further warming. Critiques of this work's methodology soon followed (12–14), but they did not preclude the existence of a strong area feedback.

Twenty years later, a recent comprehensive assessment of Earth's climate sensitivity (3) by the World Climate Research Program (WCRP), relying primarily on the observational study by Williams and Pierrehumbert (15), estimated the anvil area feedback to be -0.2 ± 0.2 Wm^{-2}K^{-1}—a range wide enough to encompass the possibility that on one end the anvil cloud area feedback is zero, and on the other end is -0.4 Wm^{-2}K^{-1}, a value large enough to make the overall cloud feedback zero, given that low cloud feedbacks are less positive than previously thought (4, 5).

Why such uncertainty in that assesment? One reason is that evidence from models were ignored because of their large intermodel spread in anvil cloud climatology and response to warming (3). Even cloud resolving models still exhibit a large spread in cloud area (16) and changes in cloud area with warming (17), likely because unconstrained microphysical parameterizations alter the proportionality between clear-sky convergence and anvil area (18, 19). And even in a study where cloud area changes are more directly imposed in general circulation models, one model shows a *decrease* in climate sensitivity whereas the other shows an *increase* (20). In other words, it is hard to make definitive conclusions based on models. Tentatively, the most recent generations of climate models (21, 22) suggest an anvil area feedback of -0.04 ± 0.06 Wm^{-2}K^{-1} (21–23), a much weaker value than that from recent observational-based assessments (3, 24).

Clearing the cloud of uncertainty. This large range of uncertainty might be whittled down by considering the *physical* constraints on anvil clouds. There is a sense that the area feedback should be small because the anvil cloud radiative effect is small (8, 25, 26). If anvils remain radiatively neutral, then no amount of change in their area could induce a cloud feedback. The simplicity of this constraint is appealing, but its explanatory power is qualitative and degree of validity unclear. How neutral must anvil clouds be for their feedback to be insignificant? What if their cloud radiative effect changes with warming? And what if anvils shrink and expose more of the Earth to the radiative effects and feedbacks of underlying low

Significance Statement

The change in tropical anvil cloud cover with warming is one of the most uncertain feedbacks when estimating the Earth's warming from increased CO_2, so we develop a simple theory to better understand and constrain it. Using satellite observations in conjunction with our theory, we show that the global mean area feedback is small because anvil clouds have little effect on Earth's energy balance in the present day. In light of our improved understanding, we more than halve the uncertainty in the anvil area feedback and reduce the overall uncertainty associated with the effect of cloud changes on global warming.

B.A.M and S.B. designed research; B.A.M. performed research. B.A.M, S.B, and J.L.D. analyzed data; and B.A.M wrote the paper.

The authors declare no conflict of interest.

[1]To whom correspondence should be addressed. E-mail: bam218@exeter.ac.uk

Table 1. ***Climatological values of tropical quantities (30° S – 30° N) used in this study.*** **All radiative quantities are evaluated at the top of atmosphere. See Climatology section for details.**

Quantity	Description	Value	Derivation
f_h	Anvil cloud area fraction	0.17	CALIPSO
f_ℓ	Low cloud area fraction	0.10	CALIPSO
T_h	Anvil temperature	221 K	ERA5
T_ℓ	Low cloud temperature	287 K	ERA5
T_s	Surface temperature	298 K	HadCRUT5
α_h	Anvil albedo	0.45	Fitted
α_ℓ	Low cloud albedo	0.45	Fitted
α_s	Surface albedo	0.13	CERES
$S^\downarrow$	Incoming shortwave radiation	398 Wm^{-2}	CERES
S_{cs}	Clear-sky absorbed shortwave	347 Wm^{-2}	CERES
R_{cs}	Clear-sky outgoing longwave	287 Wm^{-2}	CERES
C	Net cloud radiative effect	-14.8 Wm^{-2}	Fitted
C^{sw}	Shortwave cloud radiative effect	-41.8 Wm^{-2}	Fitted
C^{lw}	Longwave cloud radiative effect	27.0 Wm^{-2}	Fitted
C_h	Anvil cloud radiative Effect	-2.0 Wm^{-2}	Inferred
C_ℓ	Low cloud radiative effect	-13.4 Wm^{-2}	Inferred
$m_{\ell h}$	Cloud overlap effect	0.5 Wm^{-2}	Inferred

clouds? Is the constraint still valid?

Quantifying this "small begets small" constraint could help answer whether the WCRP lower bound on the area feedback (-0.4 $\mathrm{Wm}^{-2}\mathrm{K}^{-1}$) is realistic. It could also provide an independent method of estimating the area feedback and would be a new way to relate present day observations to climate change. This motivates the following questions aimed at sharpening this basic intuition:

- How does the area feedback scale with changes in anvil cloud cover? How important is overlap with low clouds?
- Does the area feedback depend more on the change in cloud radiative effect or its present day value?
- If the latter, can the small observed anvil radiative effect (27–32) be used to constrain the anvil area feedback?

We address these questions with a conceptual yet quantitative model of cloud radiative effects. We will show how the area feedback depends on *present day*, and thus measurable, cloud radiative effects. We will diagnose them using satellite observations and reanalysis in conjunction with our theory and use them to constrain the area feedback. We will look at the implications for climate sensitivity and revisit the original iris hypothesis (11). Finally, we will discuss how other cloud feedbacks can be studied with our framework.

Conceptualizing cloud radiative effects

We start with an idealized model of cloud radiative effects at the top of the atmosphere (TOA). Although tropical cloudiness is expected to be trimodal (33), for simplicity we will consider a domain containing two cloud types: high clouds (h) and low clouds (ℓ). Each type has a temperature T_h, T_ℓ; an optically thick cloud fraction f_h, f_ℓ; and an albedo α_h, α_ℓ (Figure 1). Mid-level clouds will be considered in our error analysis.

The TOA energy balance is $N = S - R$, where S is the absorbed shortwave radiation and R is the outgoing longwave radiation. The cloud radiative effect C is the difference in N between all-sky and clear-sky (cs) conditions, $C = N - N_{cs}$

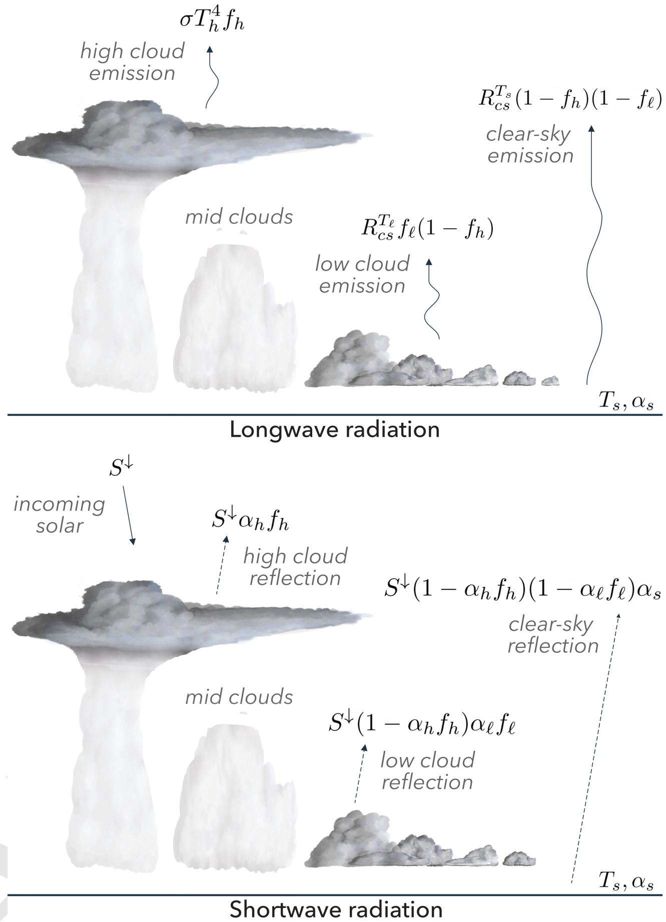

Fig. 1. *Conceptualizing cloud radiative effects.* We idealize the vertical cloud profile into two distinct layers that represent anvil clouds and low clouds with random overlap. Equations indicate the domain-averaged contribution of high clouds, low clouds, and the surface to TOA energy balance. Their sum in the longwave and shortwave is given by Equation 1 and 3, respectively. See Table 1 for symbol meanings and values.

(34). C can be decomposed into longwave and shortwave components: $C = C^{sw} + C^{lw}$.

In the longwave component, clear-sky regions with a surface temperature T_s will emit to space with an outgoing longwave radiation of $R_{cs}^{T_s}$, but a portion will be blocked by clouds. Assuming random overlap between high clouds and low clouds (35), the domain-averaged clear-sky contribution is $R_{cs}^{T_s}(1 - f_h)(1 - f_\ell)$. Low clouds are so close to the surface that we treat their emission to space like clear-sky surface emission. Their domain-averaged contribution is $R_{cs}^{T_\ell} f_\ell(1 - f_h)$. Since $R_{cs}^{T_s}$ is an approximately linear function of temperature (36), $R_{cs}^{T_\ell} \approx R_{cs}^{T_s} + \lambda_{cs}(T_s - T_\ell)$, where $\lambda_{cs} \equiv -dR_{cs}/dT_s \approx -2$ $\mathrm{Wm}^{-2}\mathrm{K}^{-1}$ is a representative value for the longwave clear sky feedback (37). We assume that high clouds are so high that they emit directly to space (38) with a value $\sigma T_h^4 f_h$. Summing these contributions, the domain-averaged outgoing longwave radiation is

$$R = R_{cs}^{T_s}(1 - f_h) + \sigma T_h^4 f_h + \lambda_{cs}(T_s - T_\ell)(1 - f_h)f_\ell, \quad [1]$$

and the longwave cloud radiative effect $-(R - R_{cs})$ is

$$C^{lw} = R_{cs} f_h - \sigma T_h^4 f_h - \lambda_{cs}(T_s - T_\ell)(1 - f_h)f_\ell. \quad [2]$$

In the shortwave component, there is an incoming solar radiation $S^{\downarrow}$, and we assume that there is no absorption except at the surface. High clouds reflect a portion $\alpha_h f_h$ back to space. The transmitted radiation then hits low clouds which reflect a portion $\alpha_\ell f_\ell$ back to space (ignoring secondary reflections with the anvils above). The transmitted radiation then hits the surface which reflects a portion α_s back out to space and absorbs the rest. Summing these contributions, the domain-averaged absorbed shortwave radiation at TOA is

$$S = S^{\downarrow}(1-\alpha_h f_h)(1-\alpha_\ell f_\ell)(1-\alpha_s). \qquad [3]$$

The TOA absorbed shortwave in clear-skies is $S_{cs} = S^{\downarrow}(1-\alpha_s)$, so the shortwave cloud radiative effect $(S - S_{cs})$ is:

$$C^{sw} = S_{cs}\big(-\alpha_h f_h - \alpha_\ell f_\ell + \alpha_h \alpha_\ell f_h f_\ell\big). \qquad [4]$$

It will prove helpful to separate the contribution of high clouds and low clouds to the net cloud radiative C. Setting $f_\ell = 0$ yields the high cloud radiative effect:

$$C_h = \big(-S_{cs}\alpha_h + R_{cs} - \sigma T_h^4\big) f_h. \qquad [5]$$

Setting $f_h = 0$ yields the low cloud radiative effect:

$$C_\ell = \big(-S_{cs}\alpha_\ell - \lambda_{cs}(T_s - T_\ell)\big) f_\ell. \qquad [6]$$

The total cloud radiative effect C in terms of each cloud is:

$$C = C_h + C_\ell + m_{\ell h}, \qquad [7]$$

where

$$m_{\ell h} = \big(S_{cs}\alpha_\ell\alpha_h + \lambda_{cs}(T_s - T_\ell)\big) f_\ell f_h, \qquad [8]$$

represents the cloud overlap masking effect. Note that $C_h \propto f_h$, $C_\ell \propto f_\ell$, and $m_{\ell h} \propto f_\ell f_h$.

The anvil cloud area feedback

Feedbacks are computed by differentiating Earth's TOA energy balance (Equation 3 minus Equation 1) with respect to the surface temperature T_s (38). The high cloud area feedback is solely due to a change in f_h, i.e. $\lambda_{\text{iris}} \equiv \partial N/\partial f_h \cdot df_h/dT_s$. After some algebra, we arrive at a remarkably simple equation:

$$\lambda_{\text{iris}} = \frac{d\ln f_h}{dT_s}\Big(C_h + m_{\ell h}\Big). \qquad [9]$$

To first order, the anvil cloud area feedback depends on the *fractional* change in anvil area with warming, multiplied by the sum of the *present day* anvil cloud radiative effect and cloud overlap effect. The logarithmic derivative is used, not only because it follows from the algebra, but also because fractional changes in cloud area are easier to interpret and bound than absolute changes—as we will soon see. The first order dependence on present-day cloud radiative effects is significant: it means they can be measured and used to constrain the feedback.

Order of magnitude considerations. In areas with large anvil cloud fractions, like the West Pacific Warm Pool, anvils have long been observed to be radiatively neutral (28), that is, $C_h + m_{\ell h} \approx 0$ Wm^{-2}. This implies a large fractional change in cloud area is required to produce a $\lambda_{\text{iris}} \sim -1$ Wm^{-2}K^{-1}, such as suggested by Lindzen et al (11). For instance, if $C_h + m_{\ell h} \sim [10, 1, 0.1]$ Wm^{-2}, then a fractional change in cloud area of $d\ln f_h/dT_s \sim -$ [10, 100, 1000] % K^{-1} would

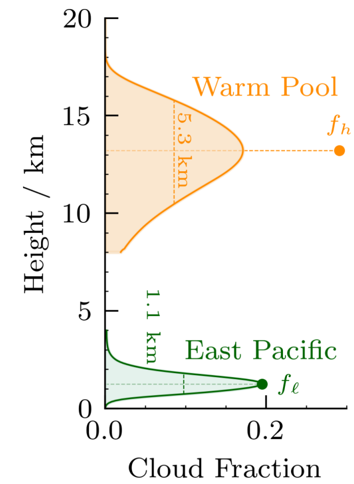

Fig. 2. *Illustration of effective cloud fraction.* The high cloud fraction profile in the Warm Pool and low cloud fraction profile in the East Pacific are from CALIPSO. The full width-half maximum and effective cloud fraction of each profile are shown. The high cloud and low cloud profiles are clipped below 8 km and above 4 km, respectively, in accordance with our detection method.

be required. Anvils, however, clearly do not shrink by more than 100% K^{-1}, so a $|C_h + m_{\ell h}| \lesssim 1$ Wm^{-2} would rule out a significant λ_{iris}, even in the most extreme case that anvils disappear entirely or double in size per degree of warming. This is the small anvil radiative effect-small area feedback hypothesis, or "small begets small", in a nutshell.

Climatology. To constrain the area feedback beyond the current estimate, a more precise diagnosis of the climatology and the change in anvil area is required. We combine monthly-mean satellite observations, surface temperature measurements, and reanalysis and re-grid all datasets onto a common 2° latitude × 2.5° longitude grid over the tropical belt (30°N−30°S) from June 2006 to December 2016.

From the CALIPSO lidar satellite dataset (39, 40), we obtain vertical profiles of cloud fraction for optical depths between $0.3 \le \tau \le 5$. This range excludes both deep convective cores and optically thin cirrus unconnected to deep convection (2). We then vertically smooth the native vertical 60 m resolution profiles with a 480 m running mean. For anvil detection, we consider ice cloud data above 8 km. For shallower clouds, we consider the sum of ice and liquid cloud fraction data below 4 km. The diagnosed cloud fractions are the absolute maximum of the profile in their respective domains, but if the identified maximum does not exceed a cutoff ($f_{\text{cut}} = 0.03$), then that region is considered to be clear-sky ($f = 0$). Our approach thus far resembles (2).

To better match the observed cloud radiative effects, we consider an effective cloud fraction $f_h = n \cdot \text{Max}(f(z))$ for high clouds. Physically, we are accounting for collapsing the high cloud profile into one level. This accounting is more important for high clouds, as their profile's full width-half maximum is ≈ 5 km (Figure 2), whereas low clouds are already localized with a full width-half maximum of ≈ 1 km (Figure 2). While n could be more rigorously derived from detailed considerations of cloud overlap (35), we opt to determine n by fitting the predicted tropical- and time-averaged longwave cloud radiative effect C^{lw} to its observed counterpart C^{lw}_{obs} from CERES (see Methods). Doing so yields a spatially and temporally constant

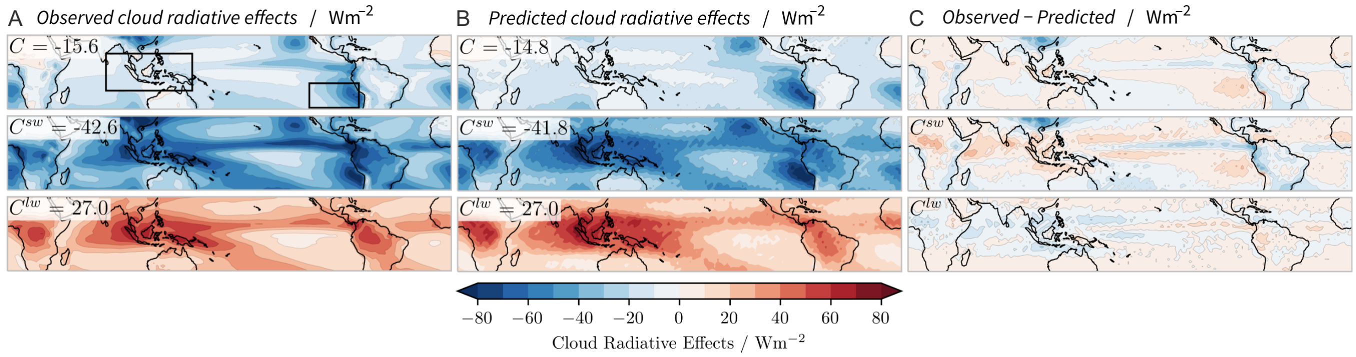

Fig. 3. *Observed net, shortwave, and longwave cloud radiative effects (C, C^{sw}, C^{lw}) from CERES compared to their predicted counterparts.* Tropical mean values are shown in the upper left of each panel. The West Pacific Warm Pool and East Pacific regions are boxed in a).

value of $n = 1.7$. This value lies between that from assuming maximum overlap between each layer of the anvil cloud, which yields $n = 1$ and random overlap, which yields $n \approx 5$.

The height of the diagnosed cloud fraction is then used to diagnose the cloud temperatures T_h, T_ℓ by selecting the corresponding atmospheric temperature in ERA5 reanalysis (41). We use the HadCRUT5 dataset (42) to diagnose the surface temperature T_s.

We use monthly mean TOA radiative fluxes, both clear-sky and all-sky, from the CERES satellite EBAF Ed4.1 product (43, 44). We diagnose the surface albedo α_s as the ratio of upwelling clear-sky shortwave radiation $S^{\uparrow}_{cs}$ to incoming shortwave radiation $S^{\downarrow}$. However, because shortwave absorption and scattering occurs in the real atmosphere, our surface albedo is more accurately characterized as the planetary clear-sky albedo (45). We diagnose the cloud albedos by assuming that they are constant, independent of space and time, and that $\alpha_h = \alpha_\ell \equiv \alpha$. (We discuss the impact of this assumption in our uncertainty analysis, see Methods.) We then fit the predicted tropical- and time-averaged shortwave cloud radiative effect C^{sw} to its observed counterpart C^{sw}_{obs} from CERES to determine α (see Methods).

We test our idealizations by comparing the observed net, shortwave, and longwave cloud radiative effects (C_{obs}, C^{sw}_{obs}, C^{lw}_{obs}) with their predicted counterparts (Figure 3), which take the spatial fields of cloud fraction, temperature, albedo, and clear-sky radiation as inputs. Our model can reproduce the spatial patterns of longwave and shortwave cloud radiative effects, although there are small deviations throughout the tropics, such as an underestimate of C in the south east of China and an overestimate of C in the eastern Pacific, next to South America (Figure 3c).

Although we fit to the tropically-averaged cloud radiative effects, anvils occur most often in the West Pacific Warm Pool (Figure 4a). There, the net cloud radiative effect is $C_{\text{obs}} = -11$ Wm^{-2}. Our model predicts $C = -10$ Wm^{-2}. Given this close agreement, we consider our model fit for the task of evaluating the anvil cloud area feedback.

The climatological values of tropical quantities used in our calculations are summarized in Table 1 and the cloud properties of interest are plotted in Figure 4. f_h is maximum in the West Pacific Warm Pool and f_ℓ is maximum along the East Pacific. Decomposing C into its contributions from different layers reveals that the net C is dominated by C_ℓ. The overlap effect $m_{\ell h}$ is much smaller by comparison and so is the

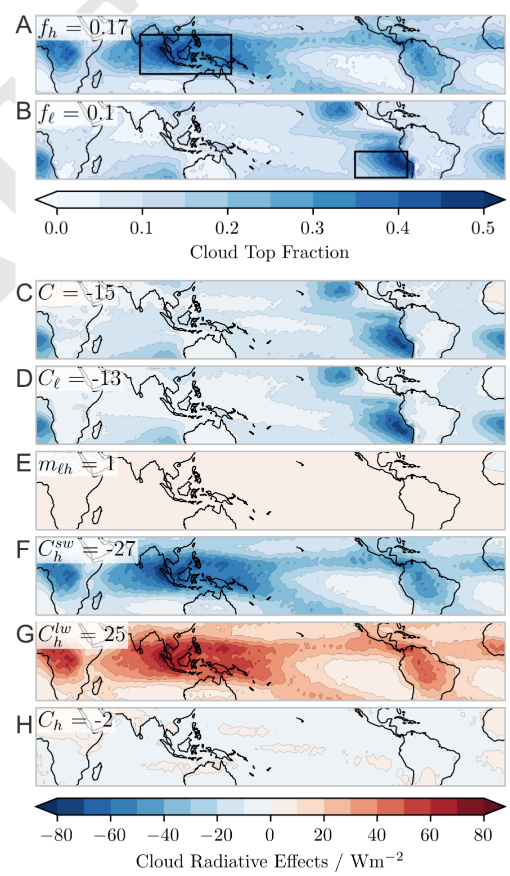

Fig. 4. *Climatological values of tropical quantities.* a) Effective anvil cloud fraction and b) low cloud fraction from CALIPSO. The West Pacific Warm Pool and East Pacific regions are boxed to indicate regions of maximum anvil and low cloud coverage, respectively. c–h) Inferred cloud radiative effects from Equations 5, 6, 8. Tropical mean values are shown in the upper left of each panel.

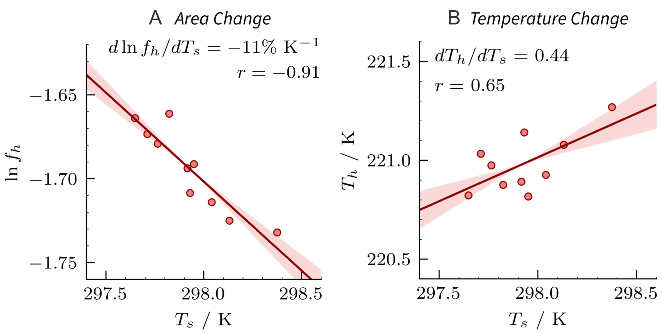

Fig. 5. *Interranual changes in anvil cloud area and temperature as a function of surface temperature.* Each point represents one year from 2006 - 2016. The slopes and correlations of the lines of best fit are shown. Errors in the slopes due to limited sampling are indicated by shading.

high cloud radiative effect C_h, which exhibits a remarkable cancellation between the shortwave and longwave components, consistent with (27–32).

Ruling out the lower bound. With these more precise values in hand, we can constrain the anvil cloud area feedback. To extend our estimates of λ_{iris} to the global average, we multiply by the area ratio of the tropics and the globe, 1/2.

$$\langle\lambda_{\text{iris}}\rangle = \frac{1}{2}\frac{d\ln f_h}{dT_s}\Big(C_h + m_{\ell h}\Big). \qquad [10]$$

The current lower bound on $\langle\lambda_{\text{iris}}\rangle$ is -0.4 Wm^{-2}K^{-1} (3), which could make the overall cloud feedback negative, a necessary ingredient for a low climate sensitivity < 1.5 K (46). Our inferred value of $C_h + m_{\ell h} = -1.5$ Wm^{-2}K^{-1} implies that $d\ln f_h/dT_s$ must be $\approx 50\%$ K^{-1} to achieve this feedback strength. In other words, anvil clouds must increase considerably in size for every degree of warming. However, even if the sign of $C_h + m_{\ell h}$ were flipped, then anvil clouds must decrease considerably in size for every degree of warming. Such small radiative effects, regardless of sign, imply correspondingly large changes in anvil area in order to produce a strong feedback.

Best estimate of the area feedback. Using the tropical mean surface temperature, we will maximize the interannual variability due to ENSO by computing annual averages of $\ln f_h$ and T_s from July to June, similar to (2). To avoid logarithmic divergences, we exclude grid cells with $f_h = 0$.

We scatter annual averages of $\ln f_h$ against T_s in Figure 5. The line of best fit for this relation gives $d\ln f_h/dT_s = -11\%$ K^{-1}, much smaller than what is required to achieve the lower bound on $\langle\lambda_{\text{iris}}\rangle$. Given this large discrepancy, the lower bound on $\langle\lambda_{\text{iris}}\rangle$ should be revised. Using Equation 10, in conjunction with our diagnosed values of $C_h + m_{\ell h} = -1.5$ Wm^{-2}, we estimate $\langle\lambda_{\text{iris}}\rangle$ to be 0.08 Wm^{-2}K^{-1}.

To calculate the uncertainty in the area feedback, $\delta\lambda$, we consider the three primary sources of error. They arise from our model ($\pm$ 0.04 Wm^{-2}K^{-1}), from limited sampling ($\pm$ 0.008 Wm^{-2}K^{-1}), and from observations ($\pm$ 0.007 Wm^{-2}K^{-1}). See Methods for details. Adding these errors in quadrature yields our best estimate of the anvil area feedback to within one standard deviation:

$$\langle\lambda_{\text{iris}}\rangle = 0.08\ \pm\ 0.05\ \mathrm{Wm^{-2}K^{-1}}. \qquad [11]$$

Our estimate for the anvil cloud area feedback is positive, but smaller in magnitude and more constrained than the observational-based WCRP estimate of -0.2 ± 0.2 Wm^{-2}K^{-1} (3) and IPCC estimate of -0.15 ± 0.2 Wm^{-2}K^{-1} (24). It is comparable in magnitude to the climate model-based estimate of -0.04 ± 0.06 Wm^{-2}K^{-1} (23). Our expression for λ_{iris} suggests this similarity might result from the strategy of tuning C^{sw} and C^{lw} in climate models to the observed global mean and spatial distribution of cloud radiative effects, as in (47, 48) for example. If models have a small C_h, their λ_{iris} will be constrained to be small and so too the spread between models, despite differences in changes of anvils with warming (17). Future work could verify such speculation.

The anvil temperature feedback

To determine the overall anvil cloud feedback, we must consider how anvils rise so as to stay nearly isothermal (49). Nearly, because anvils exhibit a proportionally higher anvil temperature (PHAT) response (50). The resulting temperature feedback is given by $\lambda_{\text{phat}} \equiv \partial N/\partial T_h \cdot dT_h/dT_s$. Applying this definition to our equation for TOA energy balance (Equation 3 minus Equation 1) and multipyling by 1/2 to estimate the global PHAT feedback, we find that

$$\langle\lambda_{\text{phat}}\rangle = -\frac{1}{2}\frac{dT_h}{dT_s}\cdot 4\sigma T_h^3 f_h. \qquad [12]$$

Since anvils emit directly to space, their temperature feedback resembles a Planckian response. Anvils warm as surface temperatures increase (50), so they emit more radiation to space and produce a negative feedback. Indeed, scattering interannual variations of T_h versus T_s suggests $dT_h/dT_s \approx 0.44$ and $T_h \approx 221$ K (Figure 5b), which yields $\lambda_{\text{phat}} = -0.09$ Wm^{-2}K^{-1}. This is in contrast to other studies, which usually consider the PHAT response to be a positive feedback (50) because it is computed relative to the case in which anvils are kept at a fixed height (51).

Using a similar method of error analysis as before (see Methods), we estimate the anvil temperature feedback to be

$$\langle\lambda_{\text{phat}}\rangle = -0.09\ \pm\ 0.07\ \mathrm{Wm^{-2}K^{-1}}. \qquad [13]$$

The anvil cloud feedback

The anvil cloud feedback is the sum of the anvil area and anvil temperature feedbacks, and it quantifies the overall radiative impact of changes in anvil clouds with warming. Summing our best estimates for each feedback and adding uncertainties in quadrature, we find that

$$\begin{aligned}\langle\lambda_{\text{anvil}}\rangle &= \langle\lambda_{\text{iris}}\rangle + \langle\lambda_{\text{phat}}\rangle \\ &= -0.01\ \pm\ 0.09\ \mathrm{Wm^{-2}K^{-1}}.\end{aligned} \qquad [14]$$

$\langle\lambda_{\text{anvil}}\rangle$ is surprisingly small. However, this result has precedence in the work of Pierrehumbert (8). They argued that the stabilizing effect of anvils on tropical climate is constrained to be small, to the extent that their radiative effect is and remains close to zero. In both their work and ours, it appears changes in anvil clouds with warming do not strongly affect climate sensitivity.

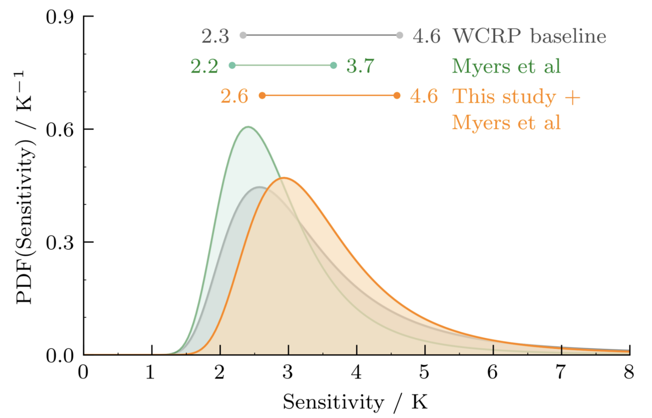

Fig. 6. *Implications for climate sensitivity.* The probability distribution for climate sensitivity (PDF), considering only process evidence, is shown for different studies. The 17th and 83rd percentile ranges are indicated.

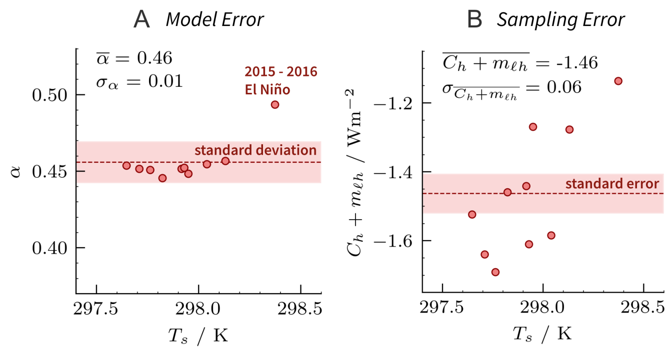

Fig. 7. *Different sources of error.* Model error is quantified by the standard deviation of the interannual variations in the tuneable parameter, the cloud albedo α. Sampling error is quantified by the standard error of the interannual variations in the diagnosed cloud radiative effects $C_h + m_{\ell h}$ (computed with $\alpha = \overline{\alpha}$).

Implications for climate sensitivity. We have ruled out a strong anvil cloud area feedback on the basis that it requires large changes in anvil area with warming that are unsupported by observations. However, even the more modest WCRP central estimate of -0.2 Wm^{-2}K^{-1} implies that anvils must change by about 25% K^{-1}, much larger than what is observed on interannual timescales. This suggests we replace the WCRP estimate of the anvil area feedback with our own. We would also like to replace the anvil temperature feedback, but λ_{phat} depends on the reference response of anvil clouds (51) and so cannot be directly compared to the WCRP estimate. We will focus on updating λ_{iris}.

Doing so changes the total cloud feedback in the WCRP study from $\lambda_{\text{cloud}} = 0.45 \pm 0.33$ Wm^{-2}K^{-1} to 0.73 ± 0.26 Wm^{-2}K^{-1}. If we incorporate recent work (4) that constrains and implies a weaker low cloud feedback (0.19 vs 0.37 Wm^{-2}K^{-1}), then $\lambda_{\text{cloud}} = 0.55 \pm 0.16$ Wm^{-2}K^{-1}. The uncertainty in cloud feedbacks is now comparable to the uncertainty in non-cloud feedbacks (3). How does this reduced uncertainty in cloud feedbacks translate to climate sensitivity?

Considering only process evidence (see Methods), the 66% likely range in the WCRP estimate of climate sensitivity is between $2.3-4.6$ K. In Myers et al (4), it is between $2.2-3.7$ K. Updating their work, we estimate it to be between $2.6-4.6$ K. Despite the decrease in uncertainty in the overall cloud feedback, the uncertainty in climate sensitivity has increased relative to Myers et al. This is a consequence of a nonlinear relationship in which a more positive overall feedback causes a larger and correspondingly more uncertain climate sensitivity (52). The rise in the lower end of the likely range is consistent with a recent assessment of climate sensitivity based on the twentieth century global energy budget (53).

Revisiting the original iris feedback hypothesis. The notion of a large negative anvil cloud area feedback originated from Lindzen et al (11), who argued that it would approximately halve the predicted climate sensitivity. Such a change corresponds to $\langle\lambda_{\text{iris}}\rangle \sim -1$ Wm^{-2}K^{-1}. We will attempt to reproduce this estimate.

Using their values: $S^{\downarrow} = 400$ Wm^{-2}, $\alpha_s = 0.13$, $\alpha_h = 0.24$, $f_h = 0.44$, we get $C_h^{sw} = -S^{\downarrow}(1-\alpha_s)\alpha_h f_h \approx -37$ Wm^{-2}. Using their "clearmoist" emission temperature $T_{\text{clear}} = 261$ K, and "cloudymoist" emission temperature $T_{\text{cloud}} = 222$ K, we get $C_h^{lw} = -\sigma(T_{\text{cloud}}^4 - T_{\text{clear}}^4)f_h \approx 55$ Wm^{-2}. Combining the two,

$$C_h^{\text{Lindzen}} \approx 18 \text{ Wm}^{-2}, \quad \text{(Lindzen et al, 2001)} \qquad [15]$$

which implies the greenhouse warming of anvils is *much* stronger than their reflective cooling. Using their change in anvil area with warming, $d\ln f_h/dT_s \approx -22\%$ K^{-1} and their idealized model configuration that confined anvil clouds to a portion, $A_h = 25\%$ of the globe, we estimate their globally averaged area feedback to be:

$$\begin{aligned}\langle\lambda_{\text{iris}}\rangle^{\text{Lindzen}} &= A_h \frac{d\ln f_h}{dT_s} C_h \\ &\approx -1.0 \text{ Wm}^{-2}\text{K}^{-1}. \quad \text{(Lindzen et al, 2001)}\end{aligned} \qquad [16]$$

Our calculation suggests that they inferred a large feedback primarily because their assumed parameters resulted in an unrealistically strong greenhouse warming from anvil clouds. Our findings are consistent with (12, 13).

Discussion

A novel feedback decomposition. Our model of cloud radiative effects is general and could be used to study other feedbacks. The total feedback is $\lambda \equiv dN/dT_s$, which can be decomposed into contributions from different cloud responses,

$$\lambda \approx \lambda_0 + \lambda_{\text{phat}} + \lambda_{\text{iris}} + \lambda_{\text{area}}^{\ell} + \lambda_{\text{warming}}^{\ell} + \lambda_{\alpha_s} + \lambda_{\alpha} \qquad [17]$$

The reference feedback, λ_0, should reflect our understanding of the climate system (54–56). For the tropical climate, it is reasonable to assume a fixed relative humidity r (57), a fixed anvil temperature (49) and area, a fixed low cloud area, a fixed temperature difference between low clouds and the surface, and a fixed surface albedo and cloud albedo. Formally expressed,

$$\lambda_0 \equiv (dN/dT_s)_{r,f_h,T_h,f_\ell,T_s-T_\ell,\alpha_s,\alpha} = \lambda_{cs}(1-f_h). \qquad [18]$$

The reference response is the anvil cloud-masked clear-sky feedback. By virtue of a fixed temperature and area fraction, anvils contribute no additional emission to space with surface warming, so they destabilize the climate relative to the clear-sky response, λ_{cs} (37, 58). Assuming $\lambda_{cs} = -2$ Wm^{-2}K^{-1} (36, 37) and $f_h = 0.17$ (Table 1) implies $\lambda_0 \approx -1.7$ Wm^{-2}K^{-1}.

Present day anvil clouds destabilize tropical climate relative to clear-skies, even though *changes* in anvil clouds with warming do not.

As already discussed, deviations from $\lambda = \lambda_0$ occur when anvil clouds warm and follow a proportionally higher anvil temperature response to produce a feedback λ_{phat}.

Our theory proposes that the anvil cloud area feedback, λ_{iris}, depends on the fractional change in cloud area, the anvil cloud radiative effect, and overlap with low clouds. Inter-model spread in these specific quantities could drive most of the spread in the anvil area feedback among climate models, thereby influencing climate sensitivity in divergent ways (20). Future work could also address the radiative impact of anvil clouds in the extratropics (59).

Low cloud area can change (4, 5), resulting in a feedback $\lambda^{\ell}_{\mathrm{area}} \equiv \partial N/\partial f_\ell \cdot df_\ell/dT_s$. In our framework, that amounts to

$$\lambda^{\ell}_{\mathrm{area}} = \frac{d\ln f_\ell}{dT_s}\Big(C_\ell + m_{\ell h}\Big). \tag{19}$$

This equation mirrors its high cloud equivalent. Thus, for both high clouds and low clouds, our theory suggests that model inter-comparison projects should consider studying the fractional change in cloud area with warming. The low cloud feedback is especially sensitive to low cloud changes because their radiative effect is large. However, cloud overlap matters little because $|m_{\ell h}| \ll |C_\ell|$ (Figure 4).

Low clouds can warm relative to the surface, contributing another feedback: $\lambda^{\ell}_{\mathrm{warming}} \equiv \partial N/\partial(T_s - T_\ell) \cdot d(T_s - T_\ell)/dT_s = -d(T_s - T_\ell)/dT_s \cdot \lambda_{cs}(1 - f_h)f_\ell$. Given that low clouds are strongly coupled to the surface ($d(T_s - T_\ell)/dT_s \approx 0$) and that $f_\ell = 0.1$, this feedback is at least an order of magnitude smaller than λ_0.

The surface albedo can change, resulting in a feedback $\lambda_{\alpha_s} \equiv \partial N/\partial \alpha_s \cdot d\alpha_s/dT_s$. In our framework,

$$\lambda_{\alpha_s} = \frac{d\ln \alpha_s}{dT_s} C_s, \tag{20}$$

where C_s is the surface albedo radiative effect, which $\equiv N - N|_{\alpha_s=0} = -S^{\downarrow}\alpha_s(1 - \alpha_h f_h)(1 - \alpha_\ell f_\ell)$. This equation reveals how clouds alter the surface albedo radiative effect and by extension the surface albedo feedback. While unimportant in the tropics, this diagnostic could be useful in studying polar regions (60) and snowball Earth (61).

The cloud albedo can change, resulting in a feedback $\lambda_\alpha \equiv \partial N/\partial\alpha \cdot d\alpha/dT_s = d\ln\alpha/dT_s \cdot (C^{sw}_h + C^{sw}_\ell + 2m^{sw}_{\ell h})$. However, α appears to change little with warming, except during an El Niño (Figure 7a).

Lingering questions. We have shown that changes in anvil cloud area with warming are not a significant feedback. If anvil cloud changes do in fact modify the tropical feedback, it must involve some other pathway. This brings us to the following open questions.

Why is the anvil cloud radiative effect so close to zero? Our results show how the anvil cloud area feedback depends on its present day radiative effect. That the radiative effect is so close to zero is essential to constraining the feedback. Although this question has been studied over the years (30, 31, 62), there is no definitive theory as to why anvil clouds are radiatively balanced and to what extent they will continue to be under climate change.

What is the feedback due to mesoscale deep-convective aggregation? Increased aggregation can reduce the anvil cloud area and dry the atmosphere (63–65). We have shown that changes in anvil cloud area are not a significant feedback, so any radiative feedback associated with aggregation is more likely to stem from humidity changes than anvil changes. There are observable changes in N and N_{cs} due to the aggregation of deep convection (63, 65), but there is no theory yet to relate them to a feedback.

Conclusions. We idealized the vertical cloud profile into two layers and then derived a simple quantitative theory for the anvil cloud area feedback. We found that the anvil cloud area feedback depends primarily on the *present day* anvil cloud radiative effect. This radiative effect is small and constrains the feedback to be small. A strong negative anvil area feedback—an essential ingredient for a low climate sensitivity—requires changes in anvil area with warming unsupported by observations. Overlap with low-level clouds does not qualitatively alter our conclusions.

We then derived and quantified the anvil cloud temperature feedback and found the overall anvil cloud feedback is extremely small. It appears that changes in anvil clouds with warming do not influence climate sensitivity.

The big picture from our work is that the anvil cloud feedback can be constrained by a simple theory that relates observations to climate change. Lingering questions in climate, such as whether mesoscale aggregation is a significant feedback, or what causes the observed reduction in absorbed solar radiation $dS/dt \approx -0.6$ Wm^{-2}decade^{-1} (66–69), might be fruitfully addressed through a similar type of physical reasoning.

This approach could provide a simple framework for interpreting which model biases influence feedbacks and climate sensitivity and which do not. For example, models might simulate too few, too bright low clouds in models (70). Will this bias their low cloud feedback? Perhaps not. If the low clouds' fractional changes with warming and their radiative effects are accurately simulated, then the model will have an unbiased low cloud feedback. Thus, our approach could provide testable hypothesis that motivate new studies and advance our understanding of models.

Such an approach has even broader implications. Communicating with the public about our confidence (or lack thereof) in clouds and climate change is hard. However, a physical theory of cloud feedbacks that can constrain, quantify, and interpret models and observations, like the one proposed here, could help clear the cloud of uncertainty.

Materials and Methods

Cloud fraction. We use the CALIPSO Lidar Satellite CAL_LID_L3_Cloud_Occurence-Standard-V1-00 data product, the same dataset used in (2). To determine the effective cloud fraction $f_h = n \cdot \mathrm{Max}(f(z))$, we first demand that n be constant with space and time. We then fit the predicted tropically- and temporally-averaged longwave radiative effect C^{lw} to its observed counterpart C^{lw}_{obs} from CERES. Given these constraints, and the inputs to Equation 2, n can be solved for as

$$n = \frac{\langle C^{lw}_{\mathrm{obs}} + \lambda_{cs}(T_s - T_\ell)f_\ell\rangle}{\langle R_{cs}\max(f(z)) - \sigma T_h^4 \max(f(z)) + \lambda_{cs}(T_s - T_\ell)f_\ell \max(f(z))\rangle}, \tag{21}$$

where $\langle\cdot\rangle$ denotes a tropical- and temporal-average.

Cloud albedo. To determine the cloud albedos α_h, α_ℓ, we first demand that they equal a common value α, and then we fit the predicted tropically- and temporally-averaged shortwave cloud radiative effect C^{sw} to equal its observed counterpart C^{sw}_{obs} from CERES. Given these constraints, and the inputs to Equation 4, the cloud albedo can be solved for as

$$\alpha = -\langle b\rangle - \sqrt{\frac{\langle b\rangle^2 - 4\langle a\rangle\langle c\rangle}{2\langle a\rangle}}, \qquad [22]$$

where $a = S_{cs} f_h f_\ell$, $b = -S_{cs}(f_h + f_\ell)$, $c = -C^{sw}_{\mathrm{obs}}$.

Uncertainty analysis for iris feedback. *Model error:* To assess the validity of our model's assumptions, we look at the interranual variations in our tunable parameter, the cloud albedo α. If our assumptions were perfect, then our model would capture the relationship between interranual variations in cloud area and TOA energy balance without having to retune α in order to make the predicted tropical mean cloud radiative effect equal its observed counterpart. In actuality, α varies from its 10-year value of $\overline{\alpha} = 0.45$ with a standard deviation of 0.01 (Figure 7). Propagating this spread in α via Equations 5 and 8 results in $\delta(C_h + m_{\ell h}) = 1.5$ $\mathrm{Wm^{-2}}$, where $\delta(\cdot)$ denotes the uncertainty in that quantity.

Another source of model error is neglecting mid-level clouds, a fairly common cloud type (33). Let's assume that emission from mid level congestus clouds (c) experience a clear-sky greenhouse effect. By symmetry with low clouds, they should contribute an additional cloud overlap masking term that appears in our expression for λ_{iris}: $m_{ch} = (S_{cs}\alpha_c\alpha_h + \lambda_{cs}(T_s - T_c))f_c f_h$. Assuming that $f_c = 0.1$, $f_h = 0.17$, $\alpha_c = \alpha_h = 0.45$, $T_c = 250$ K, $T_s = 298$ K, $S_{cs} = 347$ $\mathrm{Wm^{-2}}$, $\lambda_{cs} = -2$ $\mathrm{Wm^{-1}K^{-1}}$ yields $m_{ch} \approx -0.44$ $\mathrm{Wm^{-2}}$.

Our total model error in radiative effects is then around 1.9 $\mathrm{Wm^{-2}}$ which propagates to a feedback error of $\delta\lambda_{\mathrm{model}} = 0.05$ $\mathrm{Wm^{-2}K^{-1}}$.

Sample error: We infer a long term feedback from short term observations. The uncertainty in our estimated values due to our limited sampling is quantified as the standard error (71). Therefore, $d\ln f_h/dT_s = -10.6 \pm 1.7\%$ $\mathrm{K^{-1}}$ (Figure 5a) and $C_h + m_{\ell h} = -1.32 \pm 0.04$ $\mathrm{Wm^{-2}}$ (Figure 7b), implying $\delta\lambda_{\mathrm{sample}} = 0.007$ $\mathrm{Wm^{-2}K^{-1}}$.

Observational error: CERES TOA fluxes have a stated uncertainty of 2.5 $\mathrm{Wm^{-2}}$ (43). Assuming that the fractional uncertainty of $(C_h + m_{\ell h})$ and C are equal, then $\delta(C_h + m_{\ell h}) = (C_h + m_{\ell h}) \cdot \delta C/C = 0.25$ $\mathrm{Wm^{-2}}$. We will ignore errors in CALIPSO measurements of the cloud fraction profile, because any deviations from the true value of cloud fraction will be accounted for by changes in α. Propagating the uncertainties in $C_h + m_{\ell h}$ results in $\delta\lambda_{\mathrm{obs}} = 0.007$ $\mathrm{Wm^{-2}K^{-1}}$.

We sum these errors in quadrature to arrive at our best estimate of the anvil area feedback:

$$\langle\lambda_{\mathrm{iris}}\rangle = 0.08 \pm 0.05\ \mathrm{Wm^{-2}K^{-1}}. \qquad [23]$$

Uncertainty analysis for PHAT feedback. *Sample error*: The uncertainty in our estimated value of dT_h/dT_s is quantified as the standard error (Figure 5b). Therefore, $dT_h/dT_s = 0.44 \pm 0.18$ $\mathrm{KK^{-1}}$. This translates to an uncertainty in the feedback $\delta\lambda_{\mathrm{sample}} = 0.07$ $\mathrm{Wm^{-2}K^{-1}}$.

Observational error: Based on CALIPSO data, we estimate $T_h = 221$ K. However, Zelinka and Hartmann (72) use Cloudsat data (73) and find that $T_h = 217$ K (see their Figure 9). We will therefore assign a standard deviation of 4 K to our estimate: $T_h = 221 \pm 4$ K. This translates to an uncertainty in the feedback $\delta\lambda_{\mathrm{obs}} = 0.01$ $\mathrm{Wm^{-2}K^{-1}}$.

We sum these errors in quadrature to arrive at our best estimate of the anvil temperature feedback:

$$\langle\lambda_{\mathrm{phat}}\rangle = 0.09 \pm 0.08\ \mathrm{Wm^{-2}K^{-1}}. \qquad [24]$$

Estimating climate sensitivity. We estimate climate sensitivity by considering process evidence. We assume that uncertainty in the forcing and feedback are Gaussian and uncorrelated, so the climate sensitivity is described by the ratio distribution $\mathcal{W} = -\mathcal{N}_F/\mathcal{N}_\lambda$ as specified analytically by (74), where $\mathcal{N}_F$ is the normal distribution of values for the forcing due to a doubling of CO_2, and $\mathcal{N}_\lambda$ is the normal distribution of values for the total feedback.

To generate the WCRP baseline (3), $\mathcal{N}_F = \mathcal{N}(4.0, 0.3)$ $\mathrm{Wm^{-2}}$ and $\mathcal{N}_\lambda = \mathcal{N}(-1.30, 0.44)$ $\mathrm{Wm^{-2}K^{-1}}$ is used, where $\mathcal{N}(\mu, \sigma)$ is a normal distribution with mean μ and standard deviation σ.

To generate the Myers et al estimate (4), the WCRP low cloud feedback of $\lambda_{\mathrm{low}} = 0.37 \pm 0.22$ $\mathrm{Wm^{-2}K^{-1}}$ is replaced with $\lambda_{\mathrm{low}} = 0.19 \pm 0.07$ $\mathrm{Wm^{-2}K^{-1}}$, which results in $\mathcal{N}_\lambda = \mathcal{N}(-1.48, 0.39)$ $\mathrm{Wm^{-2}K^{-1}}$.

To generate our estimate, the Myers et al estimate of λ_{low} is kept, but the WCRP high cloud area feedback of $\lambda_{\mathrm{iris}} = -0.2 \pm 0.2$ $\mathrm{Wm^{-2}K^{-1}}$ is replaced with $\lambda_{\mathrm{iris}} = 0.08 \pm 0.05$ $\mathrm{Wm^{-2}K^{-1}}$, which results in $\mathcal{N}_\lambda = \mathcal{N}(-1.20, 0.33)$ $\mathrm{Wm^{-2}K^{-1}}$.

Data and code availability. Data and code used to generate the numbers and figures in this text will be made available in Zenodo and Github repositories upon acceptance.

ACKNOWLEDGMENTS. We thank Geet George for illustrating the clouds in Figure 1 and Marion Saint-Lu for helpful conversations throughout the project. B.M. was supported by the Franco-American Fulbright Commission. S.B. and J.L.D. were supported by EU Horizon 2020 grant agreement 820829 (CONSTRAIN)

References

1. S Bony, et al., Thermodynamic control of anvil cloud amount. *Proc. Natl. Acad. Sci.* **113**, 8927–8932 (2016).
2. M Saint-Lu, S Bony, JL Dufresne, Observational evidence for a stability iris effect in the tropics. *Geophys. Res. Lett.* **47**, e2020GL089059 (2020) e2020GL089059 10.1029/2020GL089059.
3. SC Sherwood, et al., An assessment of earth's climate sensitivity using multiple lines of evidence. *Rev. Geophys.* **58**, e2019RG000678 (2020) e2019RG000678 2019RG000678.
4. TA Myers, et al., Observational constraints on low cloud feedback reduce uncertainty of climate sensitivity. *Nat. Clim. Chang.* **11**, 501–507 (2021).
5. R Vogel, et al., Strong cloud–circulation coupling explains weak trade cumulus feedback. *Nature* **612**, 696–700 (2022).
6. V Ramanathan, W Collins, Thermodynamic regulation of ocean warming by cirrus clouds deduced from observations of the 1987 El Niño. *Nature* **351**, 27–32 (1991).
7. KM Lau, CH Sui, MD Chou, WK Tao, An inquiry into the cirrus-cloud thermostat effect for tropical sea surface temperature. *Geophys. Res. Lett.* **21**, 1157–1160 (1994).
8. RT Pierrehumbert, Thermostats, radiator fins, and the local runaway greenhouse. *J. Atmospheric Sci.* **52**, 1784 – 1806 (1995).
9. S Bony, KM Lau, YC Sud, Sea surface temperature and large-scale circulation influences on tropical greenhouse effect and cloud radiative forcing. *J. Clim.* **10**, 2055 – 2077 (1997).
10. IN Williams, RT Pierrehumbert, M Huber, Global warming, convective threshold and false thermostats. *Geophys. Res. Lett.* **36** (2009).
11. RS Lindzen, MD Chou, AY Hou, Does the earth have an adaptive infrared iris? *Bull. Am. Meteorol. Soc.* **82**, 417 – 432 (2001).
12. Q Fu, M Baker, DL Hartmann, Tropical cirrus and water vapor: an effective earth infrared iris feedback? *Atmospheric Chem. Phys.* **2**, 31–37 (2002).
13. B Lin, BA Wielicki, LH Chambers, Y Hu, KM Xu, The iris hypothesis: A negative or positive cloud feedback? *J. Clim.* **15**, 3 – 7 (2002).
14. DL Hartmann, ML Michelsen, No evidence for iris. *Bull. Am. Meteorol. Soc.* **83**, 249 – 254 (2002).
15. IN Williams, RT Pierrehumbert, Observational evidence against strongly stabilizing tropical cloud feedbacks. *Geophys. Res. Lett.* **44**, 1503–1510 (2017).
16. AA Wing, et al., Clouds and convective self-aggregation in a multimodel ensemble of radiative-convective equilibrium simulations. *J. Adv. Model. Earth Syst.* **12**, e2020MS002138 (2020) e2020MS002138 10.1029/2020MS002138.
17. CL Stauffer, AA Wing, Properties, changes, and controls of deep-convecting clouds in radiative-convective equilibrium. *J. Adv. Model. Earth Syst.* **14**, e2021MS002917 (2022) e2021MS002917 2021MS002917.
18. N Jeevanjee, Three rules for the decrease of tropical convection with global warming. *J. Adv. Model. Earth Syst.* **14**, e2022MS003285 (2022) e2022MS003285 2022MS003285.
19. H Beydoun, PM Caldwell, WM Hannah, AS Donahue, Dissecting anvil cloud response to sea surface warming. *Geophys. Res. Lett.* **48**, e2021GL094049 (2021) e2021GL094049 2021GL094049.
20. T Mauritsen, B Stevens, Missing iris effect as a possible cause of muted hydrological change and high climate sensitivity in models. *Nat. Geosci.* **8**, 8–13 (2015).
21. KE Taylor, RJ Stouffer, GA Meehl, An overview of cmip5 and the experiment design. *Bull. Am. Meteorol. Soc.* **93**, 485 – 498 (2012).
22. V Eyring, et al., Overview of the coupled model intercomparison project phase 6 (cmip6) experimental design and organization. *Geosci. Model. Dev.* **9**, 1937–1958 (2016).
23. MD Zelinka, SA Klein, Y Qin, TA Myers, Evaluating climate models' cloud feedbacks against expert judgment. *J. Geophys. Res. Atmospheres* **127**, e2021JD035198 (2022) e2021JD035198 2021JD035198.
24. P Forster, et al., Chapter 7: The Earth's energy budget, climate feedbacks, and climate sensitivity. *Intergovernmental Panel on Clim. Chang.* (2021).
25. DL Hartmann, Tropical anvil clouds and climate sensitivity. *Proc. Natl. Acad. Sci.* **113**, 8897–8899 (2016).
26. P Ceppi, F Brient, MD Zelinka, DL Hartmann, Cloud feedback mechanisms and their representation in global climate models. *WIREs Clim. Chang.* **8**, e465 (2017).

27. DL Hartmann, DA Short, On the use of earth radiation budget statistics for studies of clouds and climate. *J. Atmospheric Sci.* **37**, 1233 – 1250 (1980).
28. V Ramanathan, et al., Cloud-radiative forcing and climate: Results from the earth radiation budget experiment. *Science* **243**, 57–63 (1989).
29. EF Harrison, et al., Seasonal variation of cloud radiative forcing derived from the earth radiation budget experiment. *J. Geophys. Res. Atmospheres* **95**, 18687–18703 (1990).
30. JT Kiehl, On the observed near cancellation between longwave and shortwave cloud forcing in tropical regions. *J. Clim.* **7**, 559 – 565 (1994).
31. DL Hartmann, SE Berry, The balanced radiative effect of tropical anvil clouds. *J. Geophys. Res. Atmospheres* **122**, 5003–5020 (2017).
32. M Ito, H Masunaga, Process-level assessment of the iris effect over tropical oceans. *Geophys. Res. Lett.* **49**, e2022GL097997 (2022) e2022GL097997 2022GL097997.
33. RH Johnson, TM Rickenbach, SA Rutledge, PE Ciesielski, WH Schubert, Trimodal characteristics of tropical convection. *J. Clim.* **12**, 2397 – 2418 (1999).
34. JA Coakley, DG Baldwin, Towards the objective analysis of clouds from satellite imagery data. *J. Appl. Meteorol. Climatol.* **23**, 1065 – 1099 (1984).
35. L Oreopoulos, N Cho, D Lee, Revisiting cloud overlap with a merged dataset of liquid and ice cloud extinction from cloudsat and calipso. *Front. Remote. Sens.* **3** (2022).
36. DDB Koll, TW Cronin, Earth’s outgoing longwave radiation linear due to h₂o greenhouse effect. *Proc. Natl. Acad. Sci.* **115**, 10293–10298 (2018).
37. BA McKim, N Jeevanjee, GK Vallis, Joint dependence of longwave feedback on surface temperature and relative humidity. *Geophys. Res. Lett.* **48**, e2021GL094074 (2021) e2021GL094074 2021GL094074.
38. , *Clouds and Climate: Climate Science's Greatest Challenge.* (Cambridge University Press), (2020).
39. NASA/LARC/SD/ASDC, Calipso lidar level 3 cloud occurrence data, standard v1-00 (2018).
40. DM Winker, et al., The calipso mission: A global 3d view of aerosols and clouds. *Bull. Am. Meteorol. Soc.* **91**, 1211 – 1230 (2010).
41. H Hersbach, et al., The era5 global reanalysis. *Q. J. Royal Meteorol. Soc.* **146**, 1999–2049 (2020).
42. CP Morice, et al., An updated assessment of near-surface temperature change from 1850: The hadcrut5 data set. *J. Geophys. Res. Atmospheres* **126**, e2019JD032361 (2021) e2019JD032361 2019JD032361.
43. NG Loeb, et al., Clouds and the earth's radiant energy system (ceres) energy balanced and filled (ebaf) top-of-atmosphere (toa) edition-4.0 data product. *J. Clim.* **31**, 895 – 918 (2018).
44. NG Loeb, et al., Toward a consistent definition between satellite and model clear-sky radiative fluxes. *J. Clim.* **33**, 61 – 75 (2020).
45. TS Chen, G Ohring, On the relationship between clear-sky planetary and surfae albedos. *J. Atmospheric Sci.* **41**, 156 – 158 (1984).
46. B Stevens, SC Sherwood, S Bony, MJ Webb, Prospects for narrowing bounds on earth's equilibrium climate sensitivity. *Earth's Futur.* **4**, 512–522 (2016).
47. M Zhao, et al., The gfdl global atmosphere and land model am4.0/lm4.0: 2. model description, sensitivity studies, and tuning strategies. *J. Adv. Model. Earth Syst.* **10**, 735–769 (2018).
48. F Hourdin, et al., Lmdz6a: The atmospheric component of the ipsl climate model with improved and better tuned physics. *J. Adv. Model. Earth Syst.* **12**, e2019MS001892 (2020) e2019MS001892 10.1029/2019MS001892.
49. DL Hartmann, K Larson, An important constraint on tropical cloud - climate feedback. *Geophys. Res. Lett.* **29**, 12–1–12–4 (2002).
50. MD Zelinka, DL Hartmann, Why is longwave cloud feedback positive? *J. Geophys. Res. Atmospheres* **115** (2010).
51. M Yoshimori, FH Lambert, MJ Webb, T Andrews, Fixed anvil temperature feedback: Positive, zero, or negative? *J. Clim.* **33**, 2719 – 2739 (2020).
52. GH Roe, MB Baker, Why is climate sensitivity so unpredictable? *Science* **318**, 629–632 (2007).
53. J Chenal, B Meyssignac, A Ribes, R Guillaume-Castel, Observational constraint on the climate sensitivity to atmospheric co2 concentrations changes derived from the 1971–2017 global energy budget. *J. Clim.* **35**, 4469 – 4483 (2022).
54. G Roe, Feedbacks, timescales, and seeing red. *Annu. Rev. Earth Planet. Sci.* **37**, 93–115 (2009).
55. IM Held, KM Shell, Using relative humidity as a state variable in climate feedback analysis. *J. Clim.* **25**, 2578 – 2582 (2012).
56. N Jeevanjee, DDB Koll, N Lutsko, "simpson's law" and the spectral cancellation of climate feedbacks. *Geophys. Res. Lett.* **48**, e2021GL093699 (2021) e2021GL093699 2021GL093699.
57. R Colman, BJ Soden, Water vapor and lapse rate feedbacks in the climate system. *Rev. Mod. Phys.* **93**, 045002 (2021).
58. B Stevens, L Kluft, A colorful look at climate sensitivity. *EGUsphere* **2023**, 1–24 (2023).
59. DWJ Thompson, S Bony, Y Li, Thermodynamic constraint on the depth of the global tropospheric circulation. *Proc. Natl. Acad. Sci.* **114**, 8181–8186 (2017).
60. JE Kay, et al., Recent Advances in Arctic Cloud and Climate Research. *Curr. Clim. Chang. Reports* **2**, 159–169 (2016).
61. DS Abbot, et al., Clouds and snowball earth deglaciation. *Geophys. Res. Lett.* **39** (2012).
62. DL Hartmann, LA Moy, Q Fu, Tropical convection and the energy balance at the top of the atmosphere. *J. Clim.* **14**, 4495 – 4511 (2001).
63. I Tobin, S Bony, R Roca, Observational evidence for relationships between the degree of aggregation of deep convection, water vapor, surface fluxes, and radiation. *J. Clim.* **25**, 6885 – 6904 (2012).
64. THM Stein, CE Holloway, I Tobin, S Bony, Observed relationships between cloud vertical structure and convective aggregation over tropical ocean. *J. Clim.* **30**, 2187 – 2207 (2017).
65. S Bony, et al., Observed modulation of the tropical radiation budget by deep convective organization and lower-tropospheric stability. *AGU Adv.* **1**, e2019AV000155 (2020) e2019AV000155 10.1029/2019AV000155.
66. NG Loeb, et al., New generation of climate models track recent unprecedented changes in earth's radiation budget observed by ceres. *Geophys. Res. Lett.* **47**, e2019GL086705 (2020) e2019GL086705 2019GL086705.
67. G Datseris, B Stevens, Earth's albedo and its symmetry. *AGU Adv.* **2**, e2021AV000440 (2021) e2021AV000440 2021AV000440.
68. PR Goode, et al., Earth's albedo 1998–2017 as measured from earthshine. *Geophys. Res. Lett.* **48**, e2021GL094888 (2021) e2021GL094888 2021GL094888.
69. NG Loeb, et al., Evaluating twenty-year trends in earth's energy flows from observations and reanalyses. *J. Geophys. Res. Atmospheres* **127**, e2022JD036686 (2022) e2022JD036686 2022JD036686.
70. C Nam, S Bony, JL Dufresne, H Chepfer, The 'too few, too bright' tropical low-cloud problem in cmip5 models. *Geophys. Res. Lett.* **39** (2012).
71. JR Taylor, *An Introduction to Error Analysis: The Study of Uncertainties in Physical Measurements.* (University Science Books), 2nd edition, (1996).
72. MD Zelinka, DL Hartmann, The observed sensitivity of high clouds to mean surface temperature anomalies in the tropics. *J. Geophys. Res. Atmospheres* **116** (2011).
73. GL Stephens, et al., The cloudsat mission and the a-train: A new dimension of space-based observations of clouds and precipitation. *Bull. Amer. Meteorol. Soc.* **83**, 1771–1790 (2002).
74. DV Hinkley, On the ratio of two correlated normal random variables. *Biometrika* **56**, 635–639 (1969).